A Trajectory Controller for Kite Power Systems with Wind Gust Handling Capabilities

Manuel C. R. M. Fernandes, Gonçalo B. Silva, Luís Tiago Paiva and Fernando A. C. C. Fontes

SYSTEC–ISR, Faculdade de Engenharia, Universidade do Porto,
Rua Dr. Roberto Frias, Porto, Portugal

Keywords: Renewable Energy, Airborne Wind Energy, Kite Power Systems, Nonlinear Systems, Path-following Control, Safe Mode Control.

Abstract: In this paper, we address the generation of electrical power using Airborne Wind Energy Systems, comprising a kite connected through a tether to a generator on the ground. We design a controller to steer the kite to follow a pre-defined periodic path, which includes a production mode, a tether retrieval mode, and a safe mode capable of handling wind gusts.

1 INTRODUCTION

Electrical energy is crucial to satisfy modern human needs, while the amount of energy available is directly associated with development. Currently, the majority of electrical energy generated worldwide comes from fossil and nuclear fuels, which are now facing increasing societal concerns of environmental sustainability.

To address these problems, countries are enacting energy policies to encourage the use of renewable energies. In this context, in the last decades there has been a fast growth and development of renewable energy systems. Very recently, Portugal's total renewable energy production in March 2018 exceeded the country's electricity consumption for the month. Among the renewable energy sources, wind is an important large scale alternative. Wind energy is nowadays mainly extracted on-shore at low heights by wind turbines mounted on towers with a few dozen meters (50-200 m) and, despite the significant number, still growing, of wind farms, most of the existing wind energy remains unexploited since it is available at high altitudes and off-shore.

One of the promising technologies to exploit the stronger and more consistent high altitude and off-shore winds is Airborne Wind Energy (AWE), namely Kite Power Systems (Ahrens et al., 2013; Schmehl, 2018). These systems use a kite, with flexible or rigid wing, that is connected to a generator through a cable (tether). Most of such systems are based on exploiting crosswind kite power described by Loyd in 1980 (Loyd, 1980). The huge power that can poten-

tial be harvested from AWE systems is supported by the facts that wind speeds grow fast with height and that the aerodynamic lift is proportional to the square of the apparent wind velocity

$$\vec{F}^{\text{lift}} = {}^{1}\!/{}_{2} c_L(\alpha) A \mathbf{v}_a^2. \qquad (1)$$

Thus, the maximum power extraction is obtained when the kite flies at high speeds in direction perpendicular to the direction of the wind, which requires this trajectory to be periodic.

In a kite power system with a fixed generator on the ground, which is our case, electrical power is generated as the kite rises by the wind, which causes the cable to be unrolled and subsequently the generator to produce electricity (see Figure 1). Since the cable length is finite, when we reach that limit the cable is retrieved with a minimum energy expenditure and the process is repeated.

To automate this process and guarantee a positive net power output it is necessary to design a controller taking into account variations in wind direction and intensity, among other factors.

Using a 3D simulation model of the kite dynamics, considering all the forces acting on it, we design a controller to follow a desired path. Then we address the problem of handling wind gusts. When wind reaches a certain speed threshold, where tether force might be excessive, we activate gust mode in order to prevent damage to the kite or other components. We do this by stopping the kite reel-out (or reel-in, in case the gust occurs in recovery mode), and directing it upwards to an equilibrium inclination. We set the angle

533

Table 1: Nomenclature.

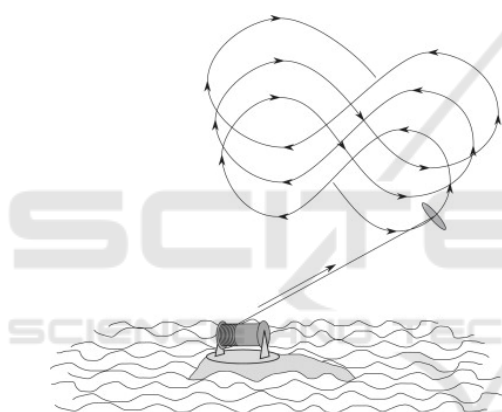|			
A	wing reference area of kite $\left[\text{m}^2\right]$	R_{GL}	rotation matrix from G to L
a_t	tether reel–out acceleration $\left[\text{m}\,\text{s}^{-2}\right]$	R_{LG}	rotation matrix from L to G
c_D	aerodynamic drag coefficient	r	tether length $[\text{m}]$
c_L	aerodynamic lift coefficient	ρ	air density $\left[\text{kg}\,\text{m}^{-3}\right]$
E	energy produced $[\text{Ws}]$	T	tether tension $[\text{N}]$
$\vec{F}^{\text{aer}}$	aerodynamic force $[\text{N}]$	$\mathbf{v}_a$	apparent wind velocity $\left[\text{m}\,\text{s}^{-1}\right]$
$\vec{F}^{\text{drag}}$	drag force $[\text{N}]$	$\mathbf{v}_w$	wind velocity $\left[\text{m}\,\text{s}^{-1}\right]$
$\vec{F}^{\text{cent}}$	centrifugal force $[\text{N}]$	v_t	tether reel–out velocity $\left[\text{m}\,\text{s}^{-1}\right]$
$\vec{F}^{\text{cor}}$	Coriolis force $[\text{N}]$	$\mathbf{u}$	control vector
$\vec{F}^{\text{lift}}$	aerodynamic lift force $[\text{N}]$	$\mathbf{x}$	state vector
$\vec{F}^{\text{inert}}$	inertial forces $[\text{N}]$	α	angle of attack $[\text{rad}]$
$\vec{F}^{\text{th}}$	tether force $[\text{N}]$	ϕ	azimuthal angle $[\text{rad}]$
g	gravitational acceleration $\left[\text{m}\,\text{s}^{-2}\right]$	β	elevation angle $[\text{rad}]$
m	mass $[\text{kg}]$	ψ	roll angle $[\text{rad}]$
P	power produced $[\text{W}]$	γ	reference tracking angle $[\text{rad}]$
$\mathbf{p}$	kite position $[\text{m}]$	τ	local tangent plane

Figure 1: Example of a kite power system in the reel-out phase (Argatov et al., 2009).

of attack to a high value, in order to have a low lift force and consequently a low tether tension force.

This technology is still not completely developed at a commercial stage. Therefore, there is a window of opportunity for new challenges, namely in the development of new controllers and continuous improvements to existing methodologies. A similar principle can be applied when the kite moves in another fluid, such as water. An example is explored in (Paiva and Fontes, 2017).

In the approach proposed here, the trajectory controller acts on the roll angle to change the kite heading direction in order to follow a moving reference point belonging a desired path (see (Prodan et al., 2015), (Caldeira and Fontes, 2010) for other approaches on path-following control). Also, a innovative wind gust mode is developed and tested. The numerical results report that such strategy allows us to handle strong wind velocities, preventing the system to crash, with-

out having to completely retract the kite.

This paper is organized as follows. In section 2, we describe a model for the kite power system. In section 3, we describe the design of a controller that allows the kite to follow a desired path. In section 4, we address the wind gust problem and how we handle it. In section 5, we provide results obtained from our simulations. In section 6, we summarize the conclusions.

2 KITE POWER SYSTEM MODEL

2.1 Coordinate System

The dynamics of the kite are modelled in a spherical coordinate system positioned at the center of mass of the kite, see (Paiva and Fontes, 2018; Canale et al., 2010). We consider three coordinate systems:

Global G: An inertial Cartesian coordinate system (x, y, z) where the origin is on the ground at the point of attachment of the tether and x is aligned according to the wind direction $\mathbf{v}_w = (v_w, 0, 0)$. The basis of this coordinate system is $(\vec{\mathbf{e}}_x, \vec{\mathbf{e}}_y, \vec{\mathbf{e}}_z)$.

Local L: A non-inertial spherical coordinate system (r, ϕ, β). The basis of this coordinate system is $(\vec{\mathbf{e}}_r, \vec{\mathbf{e}}_\phi, \vec{\mathbf{e}}_\beta)$ (Fig. 2).

Body B: A non-inertial Cartesian coordinate system attached to the kite body. The basis of this coordinate system is $(\vec{\mathbf{e}}_1, \vec{\mathbf{e}}_2, \vec{\mathbf{e}}_3)$, with $\vec{\mathbf{e}}_1$ coinciding with the kite longitudinal axis pointing forward, $\vec{\mathbf{e}}_2$ in the kite transversal axis pointing to the left
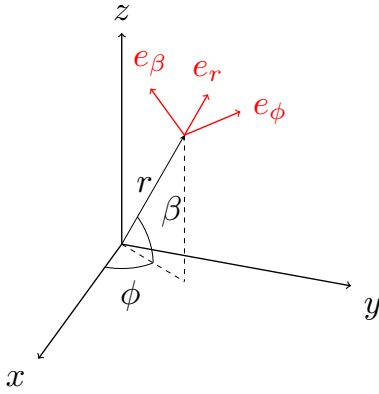
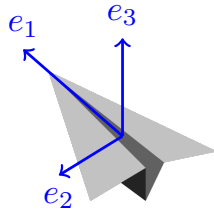Figure 2: Global and Local coordinate systems (Paiva and Fontes, 2018) .

Figure 3: Body coordinate system (Paiva and Fontes, 2018).

wing tip, and $\vec{\mathbf{e}}_3$ in the kite vertical axis pointing upwards (Fig. 3).

We consider the position

$$\mathbf{p} = \begin{bmatrix} x \\ y \\ z \end{bmatrix} = \begin{bmatrix} r\cos(\beta)\cos(\phi) \\ r\cos(\beta)\sin(\phi) \\ r\sin(\beta) \end{bmatrix},$$

the rotation matrix from L coordinate system to G

$$R_{LG} = \begin{bmatrix} \vec{\mathbf{e}}_r & \vec{\mathbf{e}}_\phi & \vec{\mathbf{e}}_\beta \end{bmatrix} =$$
$$= \begin{bmatrix} \cos(\beta)\cos(\phi) & -\sin(\phi) & -\sin(\beta)\cos(\phi) \\ \cos(\beta)\sin(\phi) & \cos(\phi) & -\sin(\beta)\sin(\phi) \\ \sin(\beta) & 0 & \cos(\beta) \end{bmatrix},$$

and the rotation matrix from G coordinate system to L

$$R_{GL} = R_{LG}^{-1} = R_{LG}^{\top}.$$

The apparent wind velocity is $\mathbf{v}_a = \mathbf{v}_w - \dot{\mathbf{p}}$. We assume that its radial component $\mathbf{v}_{a,r}$ is strictly positive and that the kite body longitudinal axis aligns naturally with the apparent wind velocity, that is $\vec{\mathbf{e}}_1 = -\mathbf{v}_a/\|\mathbf{v}_a\|$. Consider the local tangent plane τ, which tangent to a sphere centred at the origin and contains the axis $\vec{\mathbf{e}}_\phi$ and $\vec{\mathbf{e}}_\beta$.

Let ψ be the roll angle measuring rotation around the longitudinal axis ($\vec{\mathbf{e}}_1$). We consider that initially, for $\psi = 0$, $\vec{\mathbf{e}}_2$ is in the plane τ. Define $\tilde{e}_2$ to be the "unrotated" axis, with $\tilde{e}_2 = \vec{\mathbf{e}}_2$ when $\psi = 0$. We have that $\tilde{e}_2 \perp \vec{\mathbf{e}}_r$, and $\tilde{e}_2 \perp \vec{\mathbf{e}}_1$. Thus, we can then define
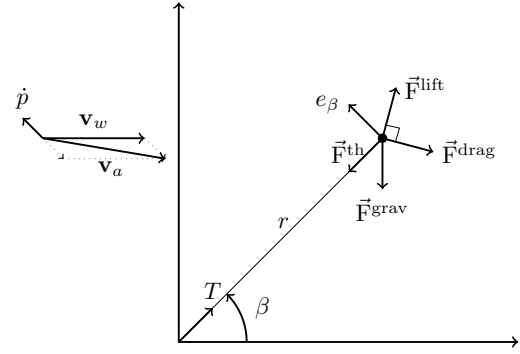

Figure 4: Forces acting on the kite (Paiva and Fontes, 2018).

$\tilde{e}_2 = \dfrac{\vec{\mathbf{e}}_r \times \vec{\mathbf{e}}_1}{\|\vec{\mathbf{e}}_r \times \vec{\mathbf{e}}_1\|}$. Finally, we consider the kite body has an anti-clockwise rotation of ψ around the $\vec{\mathbf{e}}_1$ axis: the roll angle.

We assume here that the roll angle ψ can be controlled directly. For example, in a two line kite where d is the distance between attachment points and Δr is the relative difference between the lengths of each line, we have $\sin\psi = \Delta r/d$ (cf. (Diehl, 2001)). Using Rodrigues' formula to rotate $\tilde{e}_2$ by ψ around $\vec{\mathbf{e}}_1$, we obtain

$$\vec{\mathbf{e}}_2 = \tilde{e}_2\cos\psi + (\vec{\mathbf{e}}_1 \times \tilde{e}_2)\sin\psi + \vec{\mathbf{e}}_1(\vec{\mathbf{e}}_1 \cdot \tilde{e}_2)(1-\cos\psi)$$

and finally, we define $\vec{\mathbf{e}}_3$ to be $\vec{\mathbf{e}}_3 = \vec{\mathbf{e}}_1 \times \vec{\mathbf{e}}_2$.

2.2 Acting Forces

The total force acting on the kite can be decomposed into the tether, gravity, and aerodynamical components (see Fig. 4)

$$m\ddot{\mathbf{p}} = \vec{F}^{\text{th}} + \vec{F}^{\text{grav}} + \vec{F}^{\text{aer}}(\alpha) \tag{2}$$

where

$$\vec{F}^{\text{th}} = -T\,\vec{\mathbf{e}}_r = \begin{bmatrix} -T \\ 0 \\ 0 \end{bmatrix}_L,$$

$$\vec{F}^{\text{grav}} = -mg\,\vec{\mathbf{e}}_z = \begin{bmatrix} 0 \\ 0 \\ -mg \end{bmatrix}_G = \begin{bmatrix} -mg\,\sin\beta \\ 0 \\ -mg\,\cos\beta \end{bmatrix}_L,$$

$$\vec{F}^{\text{aer}}(\alpha) = {}^1\!/_2\rho A\|\mathbf{v}_a\|^2(c_L(\alpha)\vec{\mathbf{e}}_3 - c_D(\alpha)\vec{\mathbf{e}}_1).$$

In the local coordinate system

$$\ddot{\mathbf{p}} = \begin{bmatrix} \ddot{r} \\ r\ddot{\phi}\cos(\beta) \\ r\ddot{\beta} \end{bmatrix}_L + \underbrace{\begin{bmatrix} -r\dot{\beta}^2 - r\dot{\phi}^2\cos^2(\beta) \\ 2\dot{r}\dot{\phi}\cos(\beta) - 2r\dot{\phi}\dot{\beta}\sin(\beta) \\ 2\dot{r}\dot{\beta} + r\dot{\phi}^2\cos(\beta)\sin(\beta) \end{bmatrix}_L}_{-1/m\vec{F}^{\text{inert}}}$$

$$\tag{3}$$

where the second term is $-1/m\vec{F}^{\text{inert}}$ with $\vec{F}^{\text{inert}}$ representing the inertial forces (centrifugal and Coriolis) in the local coordinate system.

Denoting the total resulting force by F, we have

$$\mathbf{F} = m \begin{bmatrix} \ddot{r} \\ r\ddot{\phi}\cos(\beta) \\ r\ddot{\beta} \end{bmatrix} = \vec{F}^{\text{th}} + \vec{F}^{\text{grav}} + \vec{F}^{\text{aer}}(\alpha) + \vec{F}^{\text{inert}}$$

(4)

We assume that the tether acceleration $\ddot{r}$ can be controlled directly by a_t. Denoting by T the tension on the tether at the base, we have $T = \mathbf{F}_r - ma_t$. We also assume that the angle of attack α and the roll angle ψ can be controlled directly, possibly by varying the differential lengths of the cable in the kite bridle. Defining the state $\mathbf{x} = \left(r, \phi, \beta, \dot{r}, \dot{\phi}, \dot{\beta} \right)$ and the control $\mathbf{u} = (a_t, \alpha, \psi)$, the dynamic equation is

$$\dot{\mathbf{x}}(t) = f(\mathbf{x}(t), \mathbf{u}(t))$$

$$= \frac{\mathrm{d}}{\mathrm{d}t} \begin{bmatrix} r \\ \phi \\ \beta \\ \dot{r} \\ \dot{\phi} \\ \dot{\beta} \end{bmatrix} = \begin{bmatrix} \dot{r} \\ \dot{\phi} \\ \dot{\beta} \\ a_t \\ \dfrac{1}{mr\cos(\beta)}\mathbf{F}_\phi \\ \dfrac{1}{mr}\mathbf{F}_\beta \end{bmatrix}.$$

(5)

2.3 Equilibrium Inclination

In strong winds or when the tether is being recoiled sufficiently fast, it is possible to maintain the kite at an equilibrium point with $\beta = \beta^\star$, $\phi = 0$, and with the angular velocities and angular accelerations equal to zero.

Consider the case of high values of the apparent wind speed, when the aerodynamical lift force is much higher than gravity. In such case

$$\vec{T} = \vec{F}^{\text{lift}} + \vec{F}^{\text{drag}}$$

and when $\dot{r} = 0$, the drag is aligned with the wind, horizontal, and the lift is vertical. Therefore

$$\beta^\star = \arctan\left(\frac{\vec{F}^{\text{lift}}}{\vec{F}^{\text{drag}}} \right) = \arctan\left(\frac{c_L}{c_D} \right)$$

When the angle of attack varies between 0° and 12° degrees, the equilibrium inclination varies between 87° and 85°. For higher angles of attack, we obtain lower lift to drag ratios and lower equilibrium inclinations. At 13.3^o we have a $\beta^* = 76^o$.

3 TRAJECTORY CONTROLLER

The total cycle consists of a production phase when the tether is reeled-out ($\dot{r} > 0$) until a maximum value of tether length r^{max} is attained. Then, follows a retraction phase when the tether is reeled-in ($\dot{r} < 0$) until a minimum value of tether length r^{min} is attained.

In order to have a predictable behaviour and optimize the energy produced by the system, the kite should track a pre-defined path. In the production phase, we define the path of Figure 5 in the spherical rectangle $\beta \in [30, 50]$, $\phi \in [-40, +40]$ degrees, where the kite should move almost cross wind. In the retraction phase, the kite goes to the vertical plane $\phi = 0$, raises the elevation angle to the equilibrium inclination, and pulls back the tether.

We define the desired production path on a (ϕ, β) coordinate system, making it independent of the tether length. We use a reference target approach to control the heading direction of the kite. Given the position of the mass-point of the kite $\mathbf{p}(\phi, \beta)$ not in the desired path, we determine the closest point to the desired path (A). Then, a reference target B is defined as the point distancing L from A in a forward direction along the path. An auxiliary vector $\vec{L}_1$ is computed between p and B (see Figure 5).

Finally, we compute the angle (γ) between the kite velocity $\dot{p}$ and $\vec{L}_1$, which serves as a reference to the desired heading direction adjustment, so that the desired path is rejoined at B. In order to control the angle (γ) towards zero, we act on the roll angle ψ using a proportional controller: $\psi(t) = K\gamma(t)$. The kite trajectory control through the heading directions, acting on the roll angle using a proportional controller has been shown to be an adequate steering command (Fagiano et al., 2014).
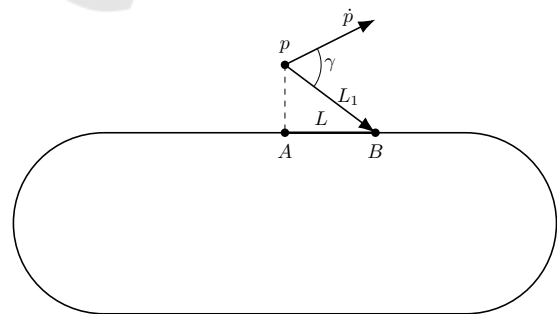
Figure 5: Trajectory Controller.

4 HANDLING WIND GUST

Although the trajectory controller system is resilient enough to support certain strong wind velocities, the resultant tether tension force might be overwhelming for the kiteline or other components. Therefore, for security purposes, a method to handle wind gusts in a robust way is crucial.

The chosen response strategy for wind velocities that we consider above the safety limit consists in elevating the kite towards the zenith, to an equilibrium inclination and centring it (i.e. $\phi=0$), by controlling the roll angle ψ (see Figure 7). Also, the tether reeling is stopped and the angle of attack is set to a high value, guaranteeing a low lift force and a high drag, stalling and decelerating the kite. The low lift force minimizes the tether tension and the stalling avoids uncontrollable movements.

When the wind velocity returns to lower values, the system resumes the normal production or retraction phase, depending on which phase was interrupted by the wind gust.

Simulation results are described in the next section.

5 SIMULATION RESULTS

We consider the simulation parameters of the kite system defined in table 2.

Table 2: Simulation Parameters.

Parameter	Value
ρ	1.2 $\mathrm{kg\,m}^{-3}$
v_w	10 $\mathrm{m\,s}^{-1}$
g	9.8 $\mathrm{m\,s}^{-2}$
m	0.7 kg
A	0.28 m^2

The aerodynamic coefficients were obtained by making a linear regression from data in (UIUC, 2018).

$$\begin{cases} c_L(\alpha) = 0.3 + 0.1\alpha, & 0 < \alpha < 12 \\ c_L(\alpha) = 9.9 - 0.7\alpha, & 12 < \alpha < 15 \end{cases}$$

$$c_D(\alpha) = 0.012 + 0.01\alpha$$

For the simulations we use the software Simulink, where we build the model presented above and design the controllers.

5.1 Fixed Tether Length

We start by simulating how the kite reacts to a wind gust when the tether is on a fixed length. As we can see in Figure 7, the kite follows the prescribed path and when the gust begins, the kite elevates to an equilibrium inclination and is centred in ϕ. When the wind velocity returns to normal values, the kite descends and resumes to follow the desired path.

As we can see in Figure 8, when the gust mode is activated, the tether force is small, as is desirable when handling strong winds. In this simulation we have first a wind velocity of 10 $\mathrm{m\,s}^{-1}$, then we increase the velocity to 30 $\mathrm{m\,s}^{-1}$, above the wind gust threshold, and finally we reduce it to 20 $\mathrm{m\,s}^{-1}$.

5.2 Complete Production Cycle

Now we see an example of a complete production cycle, with the reel-out and reel-in of the tether. As we can see on figure 9, as the kite rises and a wind gust occurs, the reeling out of the tether is stopped and the kite is elevated to an equilibrium point, returning to the trajectory as wind velocities return to lower values.

On figure 11 we can see the state variables (r, ϕ, β). We clearly see the wind gust occurring between $[200, 250]s$, as r stays constant, ϕ goes to zero and the elevation angle β rises. On figure 12 we can see the control variables, and as supposed, during the wind gust we have a high angle of attack (α) and ψ is zero since the kite is centered on $\phi = 0$. Finally, on figure 10, we can see energy is produced during the reel-out phase, and a negligible amount is spent during the reel-in phase. During the gust mode, energy is neither produced or spent.

6 CONCLUSIONS

Using a 3D dynamic simulation model of a kite power system, considering the forces acting on it, we develop here a method to control the kite to follow a pre-defined path. The prescribed path is defined only by the minimum and maximum values of ϕ and β, independently of the tether length and reel in velocity. The steering controller in the production path-following phase is based on the adjustment of the roll angle (ψ), working with a constant angle of attack. Although this procedure has shown itself robust for high wind speeds, a safety mode to avoid excessive strain on the tether and other components was developed.
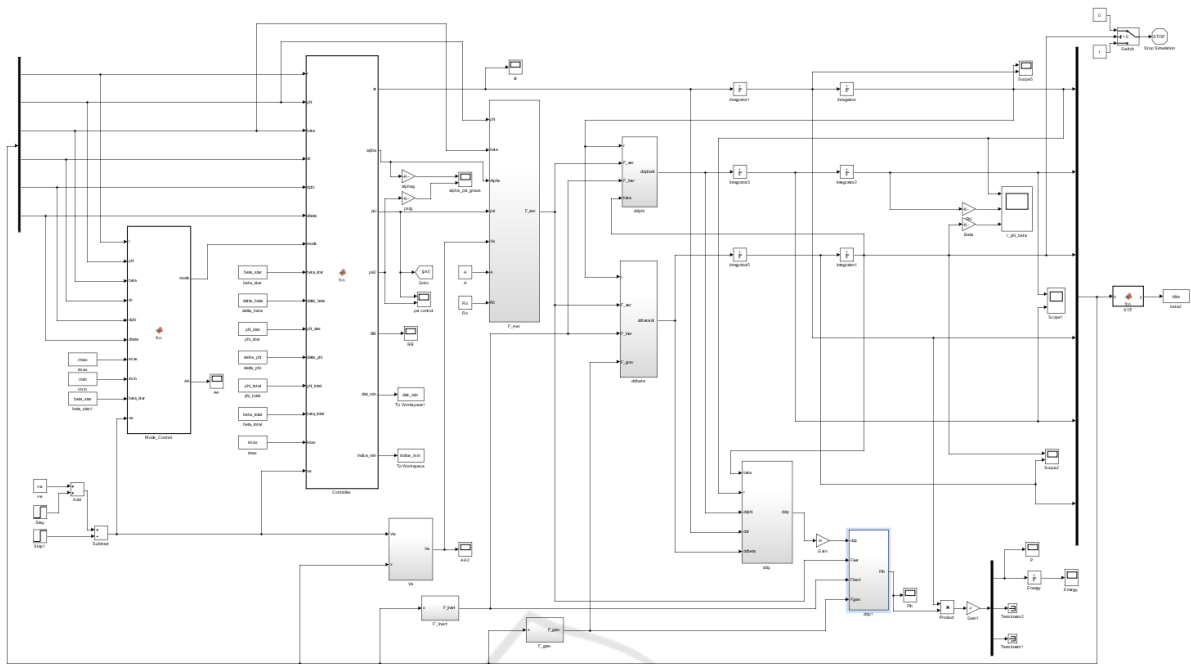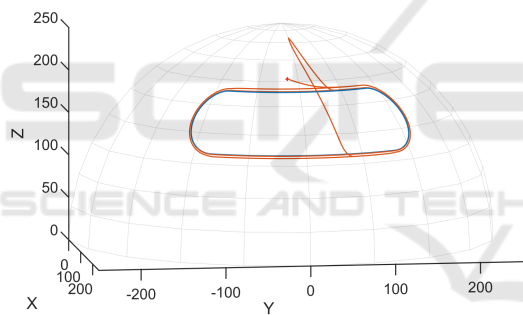
Figure 6: Simulink System.

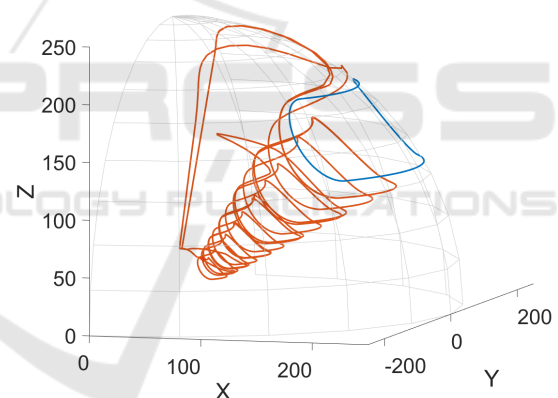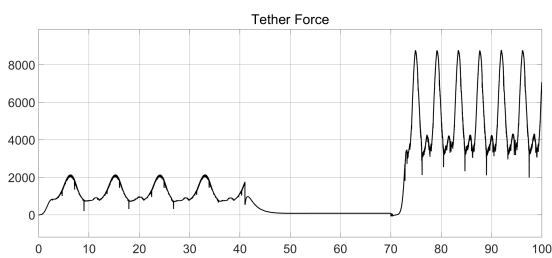

Figure 7: Kite reacting to wind gust.

Figure 8: Tether force.

The angle of attack plays an important roll to balance both drag and lift aerodynamic forces and the resultant tether tension. In the event of wind gusts, we adjust the angle of attack to an appropriate value that decreases the tether tension. Moreover, at the same time the kite is driven towards the zenith where it can handle the excessive energy contained in the wind gust.

Figure 9: Trajectory example with wind gust.

ACKNOWLEDGEMENTS

REFERENCES

Ahrens, U., Diehl, M., and Schmehl, R., editors (2013). *Airborne Wind Energy*. Green Energy and Technology.

Figure 10: Energy production.
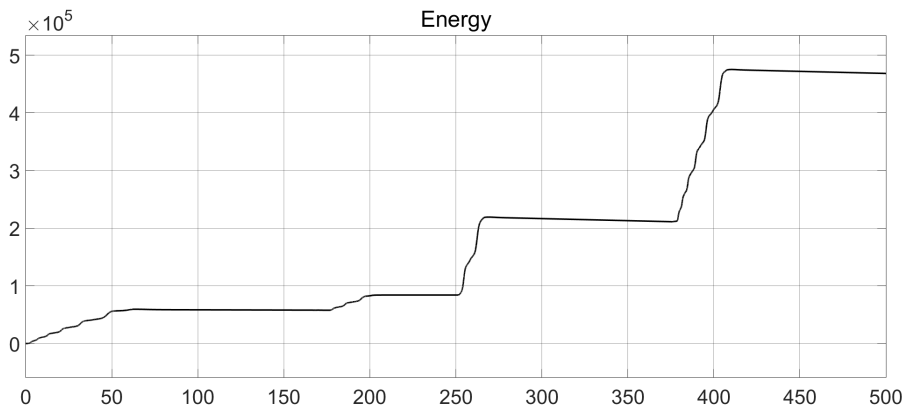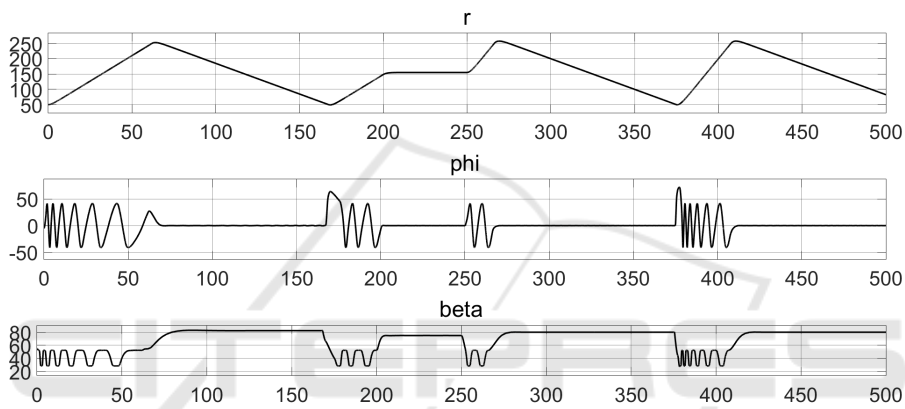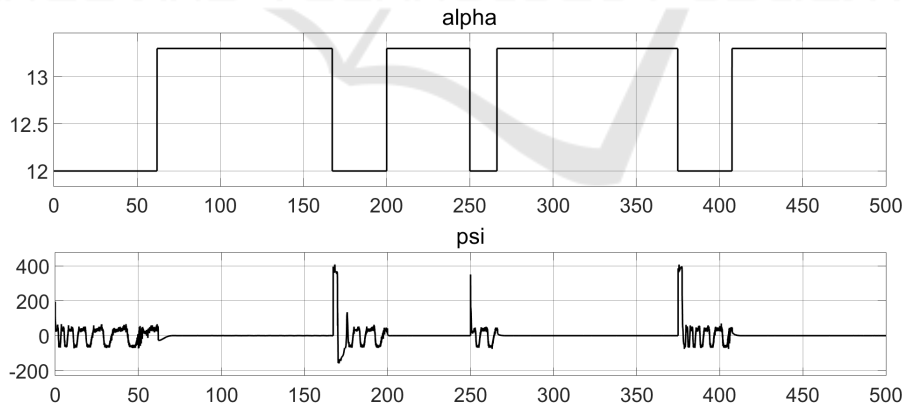

Figure 11: State variables - (r, ϕ, β).

Figure 12: Control variables - (α, ψ).

Springer Berlin Heidelberg, Berlin, Heidelberg.

Argatov, I., Rautakorpi, P., and Silvennoinen, R. (2009). Estimation of the mechanical energy output of the kite wind generator. *Renewable Energy*, 34(6):1525–1532.

Caldeira, A. C. D. and Fontes, F. A. C. C. (2010). Model predictive control for path-following of nonholonomic systems. In *Proceedings of the 10th Portuguese Conference on Automatic Control - CONTROLO 2010*,

pages 720–725, Coimbra, Portugal.

Canale, M., Fagiano, L., and Milanese, M. (2010). High Altitude Wind Energy Generation Using Controlled Power Kites. *IEEE Transactions on Control Systems Technology*, 18(2):279 –293.

Diehl, M. (2001). *Real-time optimization for large scale nonlinear processes*. PhD Thesis.

Fagiano, L., Zgraggen, A. U., Morari, M., and Khammash,

M. (2014). Automatic crosswind flight of tethered wings for airborne wind energy: modeling, control design and experimental results. *IEEE Transactions on Control Systems Technology*, 22(4):1433–1447.

Loyd, M. L. (1980). Crosswind kite power. *Journal of Energy*, 4(3):106–111.

Paiva, L. T. and Fontes, F. A. C. C. (2017). Optimal control of underwater kite power systems. In *Energy and Sustainability in Small Developing Economies (ES2DE), 2017 International Conference in*, pages 1–6. IEEE.

Paiva, L. T. and Fontes, F. A. C. C. (2018). Optimal Control Algorithms with Adaptive Time-Mesh Refinement for Kite Power Systems. *Energies*, 11(3):475.

Prodan, I., Olaru, S., Fontes, F. A. C. C., Pereira, F. L., Sousa, J. B. d., Maniu, C. S., and Niculescu, S.-I. (2015). Predictive Control for Path-Following. From Trajectory Generation to the Parametrization of the Discrete Tracking Sequences. In *Developments in Model-Based Optimization and Control*, Lecture Notes in Control and Information Sciences, pages 161–181. Springer, Cham.

Schmehl, R., editor (2018). *Airborne Wind Energy: Advances in Technology Development and Research*. Green Energy and Technology. Springer Singapore.

UIUC (2018). UIUC Airfoil Data Site. The University of Illinois at Urbana-Champaign. Acessed 2018-05-07.